

# Decaniobate: The Fruit Fly of Niobium Polyoxometalate Chemistry

May Nyman,\* Tasnim Rahman, and Ian Colliard



Cite This: *Acc. Chem. Res.* 2023, 56, 3616–3625



Read Online

ACCESS |

Metrics & More

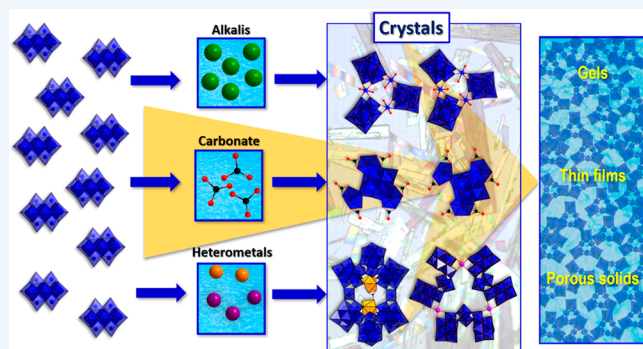
Article Recommendations

Supporting Information

**CONSPICUTUS:** Polyoxometalates (POMs, metals =  $V^{4/5+}$ ,  $Nb^{5+}$ ,  $Ta^{5+}$ ,  $Mo^{5/6+}$ , and  $W^{5/6+}$ ) can be described as molecular metal oxides. The V, Mo, and W-POMs (classic POMs) exhibit rich structural diversity with interesting redox properties, acid catalysis, inorganic ligands, and colorimetric properties and behavior. Nb and Ta POMs, while structurally similar, are generally stable only in base and redox behavior is rare, and they are synthetically far less accessible. The V, Mo, and W-POMs have been studied for well over a century, Nb-POM chemistry has emerged in the last 20 years, and Ta-POM chemistry is yet to see consistent and significant advances. Early and current success in Nb-POM chemistry is owed mainly to hydrothermal synthesis, which is wholly unsatisfying, given the black box nature of this technique.

For the last 5 years and as summarized in this Account, we have exploited decaniobate,  $[Nb_{10}O_{28}]^{6-}$  ( $Nb_{10}$ ), as a foundation to perform room-temperature, nearly pH-neutral manipulations of Nb-POM solutions.  $Nb_{10}$  with a rare neutral self-buffering pH, responds to any interactions with electrolytes (specifically oxoanions and metal cations) by undergoing transformations, leading to new topologies. The ease of  $Nb_{10}$  transformation yielding new generations of Nb-POMs, akin to an inorganic analogue of biological model organisms such as the fruit fly, inspired the title of this Account. The common building unit born from the disassembly of  $Nb_{10}$  is  $[Nb_7O_{20}(OH, H_2O)]^{(5-7)-}$ , and the hydroxyl/aqua ligands provide reactivity for linking via condensation reactions, ligand exchange, heterometals, or oxoanions. We can coax these newly assembled Nb-POMs (detected by small-angle X-ray scattering, SAXS) to crystallize via the usual methods of vapor diffusion, salting out, and reduced temperature, and the single-crystal X-ray diffraction structures are valuable for understanding reaction mechanisms to fine-tune control and yield a landscape of topologies and compositions. Beyond providing an opportunity to comprehend and diversify POM chemistry, the reactivity of  $Nb_{10}$  yields highly soluble (i.e.,  $>2$  M Nb), nearly neutral aqueous solutions of niobium, ideal for the solution-phase deposition of thin films, demonstrated with  $LiNbO_3$ ,  $(Na, K)NbO_3$ ,  $Nb_2O_5$ , and heterometal-doped  $Nb_2O_5$ . The obtained films are cohesive and smooth, enabled by the tendency of these solutions to gel if simply evaporated quickly.

Per our current endeavors, this gelation behavior provides an opportunity to develop new soft, flexible materials including inorganic networks, organic–inorganic networks, and porous solids and explore their material properties including base catalysis and sorption (i.e.,  $CO_2$ ). Nb-POM (and Ta-POM) discovery and implementation of properties is far from complete. While heterometal (d and f element) substitution is easy with classic POMs, imparting a whole host of functions (tuned luminescence, catalysis, electroactivity, etc.), it remains a challenge with Nb-POMs due to pH incompatibility with most heterometals. This grand challenge that defies fundamental aqueous behavior of metal cations requires the creation of liquid mixtures that include polymer and/or ionic liquid components, and the creation of such reaction media can impact synthesis beyond POM chemistry. The goal of this Account is to describe the recent advances in Nb-POM chemistry, afforded by the  $Nb_{10}$  “fruit fly”, and to also provide insight into the next large steps needed to advance Nb-POM chemistry.



## KEY REFERENCES

- Sures, D.; Segado, M.; Bo, C.; Nyman, M. Alkali-Driven Disassembly and Reassembly of Molecular Niobium Oxide in Water. *J. Am. Chem. Soc.* 2018, 140, 10803–10813 [10.1021/jacs.8b05015](https://doi.org/10.1021/jacs.8b05015).<sup>1</sup> Here we first discovered the conversion of  $Nb_{10}$  to larger clusters via the  $Nb_7$  intermediate simply by the addition of alkali chloride, and we explained the reaction pathway with computation.
- Rahman, T.; Martin, N. P.; Jenkins, J. K.; Elzein, R.; Fast, D. B.; Addou, R.; Herman, G. S.; Nyman, M.

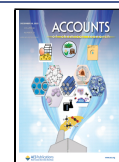
$Nb_2O_5$ ,  $LiNbO_3$ , and  $(Na, K)NbO_3$  Thin Films from High-Concentration Aqueous Nb-Polyoxometalates. *Inorg. Chem.* 2022, 61, 3586–3597 [10.1021/acs.inorgchem.2c00597](https://doi.org/10.1021/acs.inorgchem.2c00597)

Received: September 13, 2023

Revised: November 6, 2023

Accepted: November 7, 2023

Published: November 28, 2023



chem.1c03638.<sup>2</sup> In this paper, we exploit the gelation behavior of high-concentration, near-neutral Nb-POM solutions for the deposition of niobate thin films.

- Amiri, M.; Martin, N. P.; Feng, C. L.; Lovio, J. K.; Nyman, M. Deliberate Construction of Polyoxoniobates Exploiting the Carbonate Ligand. *Angew. Chem. Int. Edit* 2021, 60, 12461–12466 10.1002/anie.202017367.<sup>3</sup> This paper exemplifies how carbonate-ligated (Ln-substituted) Nb-POMs can be constructed from Nb<sub>10</sub> despite the general insolubility of Ln under neutral to alkaline conditions.

## INTRODUCTION

In 2009, George Christou dubbed the Mn<sub>12</sub>-acetate cluster the “Drosophila” of single-molecule magnetism (SMM).<sup>4</sup> Drosophila is the common fruit fly used widely in biological research, and Christou’s reference attests to the importance of the Mn<sub>12</sub> family of compounds in understanding SMM behavior. Borrowing from Christou, here we are calling decaniobate, [Nb<sub>10</sub>O<sub>28</sub>]<sup>6-</sup> (Nb<sub>10</sub>), the fruit fly of Nb-polyoxometalate (Nb-POM) chemistry due to its simplicity and its ease of manipulation to “spawn offspring” and diversify generations of Nb-POM fragments that assemble into new cluster topologies. Our fundamental research of the last 5 years that has focused on Nb<sub>10</sub> has revealed behavior different from classical POM chemistry (classical means V, Mo, and W POMs). With Nb<sub>10</sub>, we observe alkali countercations driving synthesis reactions<sup>1</sup> rather than merely spectating and governing solubility.<sup>5</sup> Nb<sub>10</sub> has given us a foundation for benchmarking and controlling assembly processes that are the heart of classic POM chemistry, but largely missing from Nb-POM chemistry. Starting in 2002,<sup>6</sup> Nb-POM chemistry has mostly relied on the blind and uninformed process of hydrothermal synthesis for compositional and topological diversification. Yet applications in nerve agent degradation, H<sub>2</sub> evolution, and other catalytic reactions arose from the increased diversification of Nb-POM chemistry.<sup>7–9</sup> Reviewed here, the manipulations of Nb<sub>10</sub> to diversify the form and function of Nb-POMs are conducive to studying reaction pathways and embody the principles of sustainable chemistry. All experiments are performed in water at mild pH with minimal electrolytes and at room temperature. This approach has created a canvas for understanding and controlling reactivity to diversify this burgeoning family of molecular metal oxides.

## INTRODUCTION TO THE POLYOXOMETALATE (POM) FAMILIES

Polyoxometalates (POM) are anionic metal-oxo clusters of the early d<sup>0</sup> transition metals that can form stable double bonds with oxo ligands. These are also known as “yl-” (M=O) complexes (i.e., group V vanadyl, niobyl, and tantalyl and group VI molybdyl and tungstyl). As pentavalent and hexavalent cations, the POM-forming metals are large enough and charge-dense enough to accommodate the multiple oxo-bonding that terminates metal-oxide cores and allows their manipulation in water without any additional ligation. This means that they are essentially water-soluble fragments of metal oxides, important for understanding processes at water-metal oxide interfaces.<sup>10</sup>

### Acidic POMs

The POM chemistries of Nb and Ta vs V, Mo, and W have similarities in topologies but differ vastly in synthetic approach.

Simply put, the synthesis of polyoxovanadates, polyoxomolybdates, and polyoxotungstates starts with an aqueous solution of the oxoanion (i.e., VO<sub>4</sub><sup>3-</sup>, MoO<sub>4</sub><sup>2-</sup>, or WO<sub>4</sub><sup>2-</sup>) that has a self-buffering pH of ~12, followed by acidification and isolation by counterion addition. Nuclearity and topology are controlled by pH, inclusion of heterometals and oxoanion templates, concentration, temperature, countercations, redox chemistry, etc., where the countercation is crucial in the crystallization of pure-phase POM clusters. The Keggin ion topology, first structurally described in 1933, remains the cornerstone of Mo-POM and W-POM chemistry, in addition to its derivatives and fragments. This chemistry, including its history,<sup>11</sup> has been described in several recent reviews.<sup>12,13</sup> While V-POM chemistry was developed with a similar synthetic approach, its smaller cationic radius leads to different topologies including rings and capsules, respectively featuring tetrahedral and square-pyramidal vanadium.<sup>14</sup> Mo-POM chemistry also features very large capsules, including partial reduction to Mo<sup>V/IV</sup>.<sup>15</sup> Even within these similar POM families, V, Mo, and W exhibit noteworthy differences based on redox potential, size, and charge.

### Basic POMs

Because the NbO<sub>4</sub><sup>3-</sup> and TaO<sub>4</sub><sup>3-</sup> species do not exist, not even in a highly basic solution, the synthetic approach to their POMs is necessarily different and historically quite challenging. Any tantalum or niobium precursor (i.e., MCl<sub>5</sub>, M<sub>2</sub>O<sub>5</sub>; M = Nb, Ta) is difficult to dissolve (especially Ta) and may require heating and/or a highly basic solution. Moreover, the specific AOH is important, where the solubility of Nb/Ta increases (qualitative observation): A<sup>+</sup> = NH<sub>4</sub> ≈ Li < Na ≪ K ≈ Rb < Cs < TMA (TMA = tetramethylammonium).<sup>5,16</sup> Under these highly alkaline conditions, Nb speciation is predominantly the Lindqvist ion (first structurally described in 1980<sup>17</sup>), [H<sub>x</sub>M<sub>6</sub>O<sub>19</sub>]<sup>(8-x)-</sup> (x = 0–3,<sup>18</sup> Nb<sub>6</sub> or Ta<sub>6</sub>, Figure 1), and crystallizes out as such,<sup>19–21</sup> without evidence for smaller mononuclear or polynuclear species. The early syntheses of M<sub>6</sub> exploited a solid-state flux of alkali hydroxide and M<sub>2</sub>O<sub>5</sub>,<sup>22</sup> and this approach is still used in more recent studies.<sup>23</sup> In 2006 and 2007, we reported the first all-aqueous routes to Nb<sub>6</sub><sup>19</sup> and Ta<sub>6</sub><sup>24</sup> respectively, using hydrous niobia and tetraperoxotantalate, which were adaptable to the use of different alkali countercations (later including TMA<sup>20</sup> and Li<sup>25,26</sup>). This also led to the recognition of the unusual solubility trend of higher solubility with more extensive ion pairing of the large alkali countercations K, Rb, and Cs.<sup>21,27</sup>

POM chemistry of Mo, W, and V was thriving at the end of the 20th century with advances in structural diversity and function. Applications exploiting rich redox behavior, supramolecular assembly, interactions with biomolecules, and POMs as inorganic ligands were summarized in a 1998 *Chemical Reviews* special issue.<sup>28</sup> Currently, these applications continue to grow, with a focus on emergent societal issues of clean energy production,<sup>29,30</sup> energy storage,<sup>31–33</sup> and health sciences.<sup>34</sup> Concurrently in the 20th century, Nb/Ta POM chemistry was largely limited to the Lindqvist ion (Nb<sub>6</sub>) and the substitution of Nb into W-POM clusters. The latter is tricky, and required temporarily stabilizing and solubilizing Nb species (i.e., with peroxide ligands) due to the acidic conditions in which W-POMs assemble and Nb/Ta oxides precipitate.<sup>35–37</sup> There were a few early examples of the polydentate complexation of metal cations with Nb<sub>6</sub>/Ta<sub>6</sub>, citing its highly charged anionic surface as a driving force.<sup>38,39</sup>

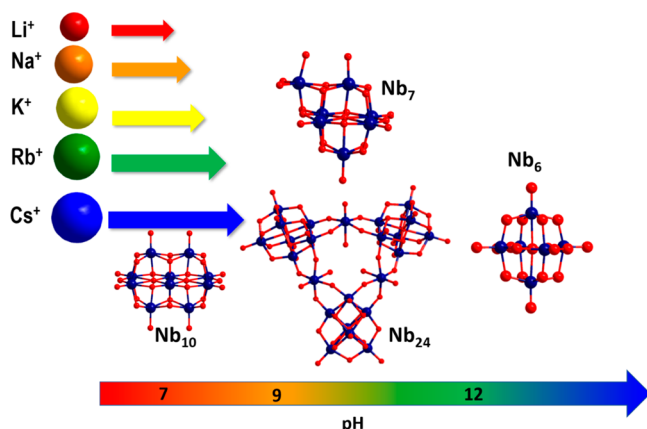


**Figure 1.** Overview of the reactivity of decaniobate,  $\text{Nb}_{10}$ ,  $[\text{Nb}_{10}\text{O}_{28}]^{6-}$ .  $\text{Nb}_{10}$  undergoes disassembly in water simply by adding alkali salts. The major product of disassembly is  $\text{Nb}_7$ , which stabilizes by the formation of  $\text{Nb}_{24}$ , a ring of three  $\text{Nb}_7$ 's linked by  $\text{H}_2\text{O}=\text{Nb}=\text{O}$  monomers. The reaction rate increases with increasing alkali size, highlighting the direct role of the alkalis in this reaction. The self-buffering pH of these reaction solutions increases from 7 to  $\sim 11.5$ , from the creation of terminal oxo ligands that become protonated. The reaction can also be driven by increasing the pH to this range. However, even when buffered at neutral pH, alkalis alone can drive this reaction. If the pH is increased further, i.e., to 12.5, the common  $\text{Nb}_6$  (Lindqvist ion) forms via removal of the addenda Nb-octahedron of  $[\text{Nb}_7\text{O}_{20}(\text{OH}, \text{H}_2\text{O})_2]^{(5-7)-}$ ,  $\text{Nb}_7$ . (Adapted with permission from ref 47, copyright (2019) Wiley-VCH Verlag GmbH&Co. KGaA.)

The isolation of these complexes faces the complementary challenge of the aforementioned, namely, that most metal cations are not soluble under the alkaline conditions in which

$\text{Nb}/\text{Ta-POMs}$  are stable, and this is the crux of enriching and developing  $\text{Nb}/\text{Ta-POM}$  chemistry to the extent of the V, Mo, and W POMs. Michael Pope, one of the pioneers of POM chemistry,<sup>39</sup> recognized this along with the complexation ability of the highly charged  $\text{Nb}$ -POMs. He cited the removal of Tc from alkaline nuclear wastes as a motivating factor to synthesize and crystallize nonradioactive  $\text{Re}/\text{Mn}-\text{Nb}_6$  and  $\text{Re}/\text{Mn}-\text{Ta}_6$  complexes.<sup>39</sup> More recently, we and others have synthesized  $\text{Nb}$ -POMs complexing base-insoluble transition metals<sup>40,41</sup> and lanthanides,<sup>3,42</sup> but these crystals are usually obtained as minor components and low yields mixed with oxide precipitates, and further ligation of the heterometal is required to enable solubility under alkaline conditions.

### Development of $\text{Nb}$ -POM Chemistry in the 21st Century

In 2002,<sup>6</sup> we reported that the hydrothermal processing of relatively mildly alkaline solutions ( $\text{pH} \approx 9.5-12$ ) in the presence of heterometals could yield  $\text{Nb}$ -POM geometries other than  $\text{Nb}_6$  (which are stable in highly alkaline solutions, i.e.,  $\text{pH} 12-14$ ), and this was the first recognition of the  $\text{Nb}$  Keggin ion<sup>43</sup> and its derivatives.<sup>44-46</sup> The majority of reported  $\text{Nb}$ -POM syntheses to date exploit hydrothermal processing as a means to dissolve  $\text{Nb}$  (and heterometals) under lower-pH conditions where the ubiquitous  $\text{Nb}_6$  species do not dominate. While this approach has been fruitful in discovering new  $\text{Nb}$ -POM topologies and applications, it is neither efficient nor satisfying in invoking control that leads to reproducible chemistries and the elucidation of reaction pathways.

### Discovery of $\text{Nb}_{10}$ Aqueous Reactivity

Decaniobate ( $\text{Nb}_{10}$ , Figure 1), isostructural with the well-known decavanadate, was crystallized from methanol ( $\text{Nb}$ -alkoxide solution) and structurally described in 1977.<sup>48</sup> This

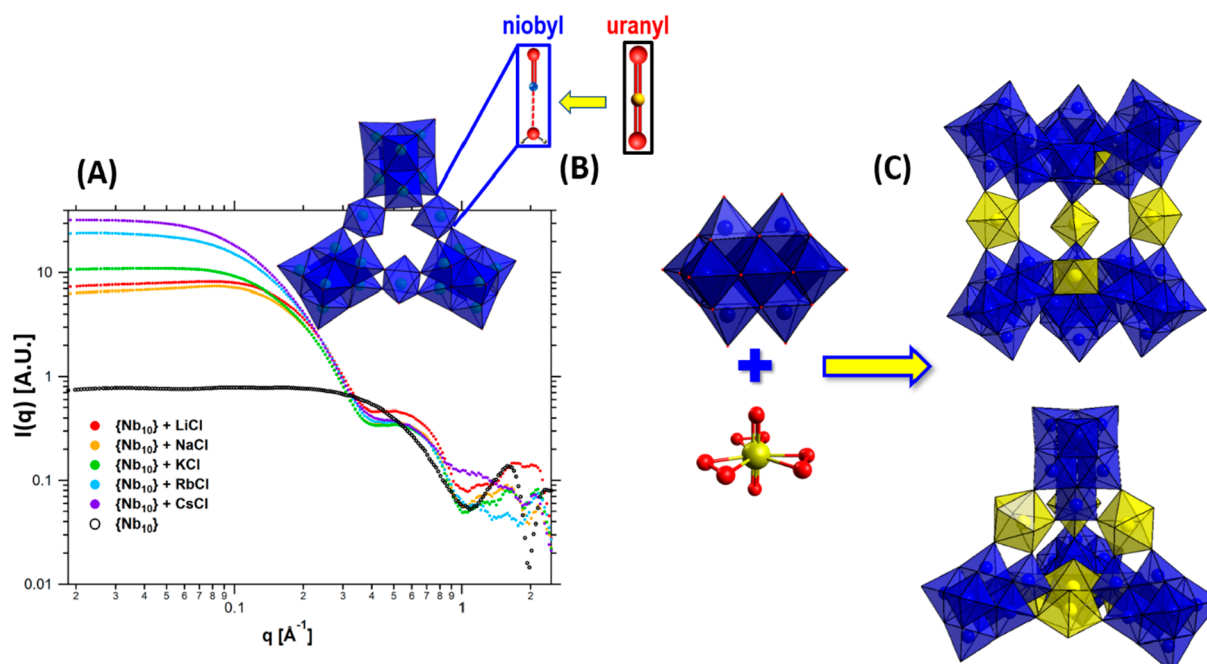


**Figure 2.** (A) SAXS of  $\text{Nb}_{10}$  (black) and  $\text{Nb}_{10}$  with added alkali chlorides showing a speciation change that suggests the formation of  $\text{Nb}_{24}$ . (B) Hypothesis to replace labile niobyl ( $\text{H}_2\text{O}=\text{Nb}=\text{O}$ ) with stable uranyl ( $\text{O}=\text{U}=\text{O}$ ) to promote crystallization. (C) Successful replacement of niobyl by uranyl in  $\text{Nb}_{24}$  clusters (using uranyl triperoxide),  $[(\text{UO}_2)(\text{H}_2\text{O})_3\text{Nb}_{46}(\text{UO}_2)_2\text{O}_{136}\text{H}_8(\text{H}_2\text{O})_4]^{24-}$  (top) and  $[(\text{Nb}_7\text{O}_{22}\text{H}_2)_4(\text{UO}_2)_7(\text{H}_2\text{O})_6]^{22-}$  (bottom). Yellow polyhedra are uranyl; blue polyhedra are niobium. (Panel A is adapted with permission from ref 1, copyright (2018) American Chemical Society. Panel C is adapted with permission from ref 47, copyright (2019) Wiley-VCH Verlag GmbH&Co. KGaA.)

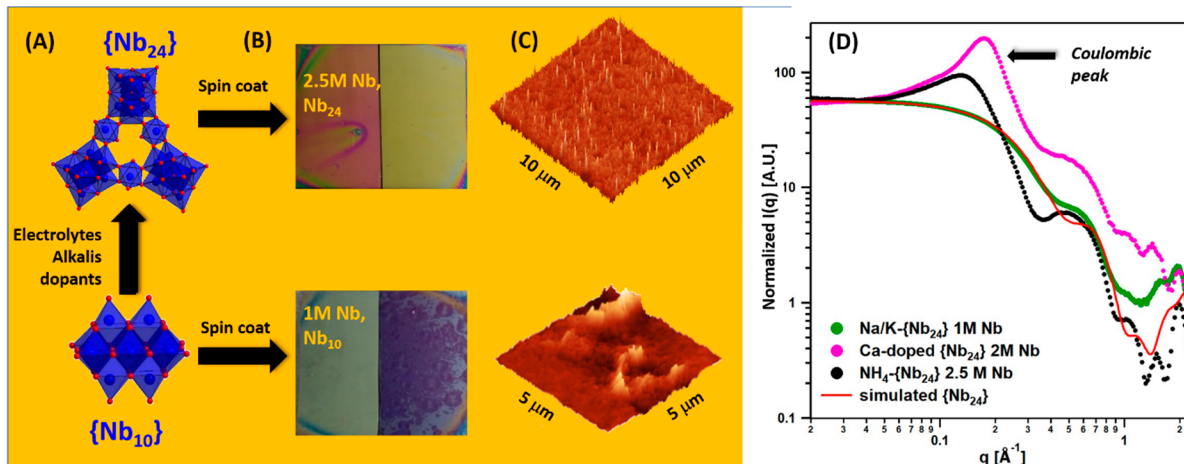


**Figure 3.** (A) Illustrated approaches to preparing high-concentration aqueous (near-neutral)  $\text{Nb}_{24}$  solutions from  $\text{Nb}_{10}$ . (B) Photographs of  $\text{Nb}_2\text{O}_5$  thin films deposited from 2.5 M Nb,  $\text{NH}_4^+$ - $\text{Nb}_{24}$  solution (top) and 1.0 M Nb,  $\text{Nb}_{10}$  solution (bottom) on silicon wafers. (Left) Deposited and soft-baked ( $200^\circ\text{C}$ ). (Right) Annealed ( $650^\circ\text{C}$ ). (C) AFM images of  $\text{Nb}_2\text{O}_5$  thin films from  $\text{NH}_4^+$ - $\text{Nb}_{24}$  solution (top) and 1.0 M Nb,  $\text{Nb}_{10}$  solution (bottom). (D) SAXS of select high-concentration  $\text{Nb}_{24}$  solutions for thin film deposition. While the Na/K- $\text{Nb}_{24}$  solution (1.0 M Nb, for KNN deposition) matches the simulated SAXS for  $\text{Nb}_{24}$ , the  $\text{Nb}_{24}$  solutions prepared from contact with poorly soluble CaOH and ammonium hydroxide both exhibit huge Coulombic peaks that indicate high concentration ( $\text{NH}_4^+$ - $\text{Nb}_{24}$ , 2.5 M Nb) and/or minimal shielding electrolytes (Ca-doped  $\text{Nb}_{24}$ , 2.0 M Nb). (Figure adapted with permission from ref 2, copyright (2022) American Chemical Society.)

chemistry was not explored further until 2001, when Marek<sup>49</sup> explained that  $\text{Nb}_{10}$  is too soluble in methanol, and he was able to develop a reliable synthesis using ethanol instead. Further studies by Villa<sup>50</sup> showed that  $\text{Nb}_{10}$  is stable only around neutral pH. We considered this, along with  $\text{Nb}_{10}$ 's high solubility in methanol, likely owed to its TMA counteraction and lower anionic charge ( $[\text{Nb}_{10}\text{O}_{28}]^{6-}$ ), an opportunity to expand Nb-POM chemistry by including heterometals in a more controlled manner. We initiated in-depth studies of  $\text{Nb}_{10}$  around 2016 by first attempting to crystallize  $\text{Nb}_{10}$  with different alkali counteractions from water. To our surprise, we found that  $\text{Nb}_{10}$  was not stable in the presence of alkalis, even when buffered near neutral pH.<sup>1</sup> Small-angle X-ray scattering (SAXS) of  $\text{Nb}_{10}$  dissolved in water with alkali chlorides showed evolution to much larger, nonspherical Nb-POMs with extremely high solubility and a tendency to gel instead of crystallize (Figure 2A). Moreover, the rate of this evolution increased considerably in the order of  $\text{Li} < \text{Na} < \text{K} < \text{Rb} < \text{Cs}$ , as did the size of the dissolved species (noted by increasing intensity and shift of the Guinier elbow, the curved part of the spectrum, from  $q \approx 0.1\text{--}0.2 \text{\AA}^{-1}$  to lower  $q$ ). Based on these rate data and the inability to suppress the reaction if the pH is buffered at neutral, this study provided the first direct evidence that alkali counteractions, often considered mere spectators, can in fact drive the speciation of metal-oxo clusters in water. Although these highly soluble clusters were reluctant to crystallize, we modeled SAXS data for suspect clusters and hypothesized with reasonable certainty that the dominant cluster form in these solutions is  $[\text{H}_x\text{Nb}_{24}\text{O}_{72}]^{(24-x)-}$ ,  $\text{Nb}_{24}$ , which we had isolated 10 years prior with  $\text{Cu}^{\text{II}}(\text{en})_2$  ( $\text{en}$  = ethylenediamine) complexes.<sup>51</sup> In this case, SAXS was our primary evidence for the dominance of  $\text{Nb}_{24}$  in these solutions since the typically-used POM solution characterization methods were not useful. For example, (1) in our experience,  $^{93}\text{Nb}$  NMR of Nb-POMs produces only broad overlapping peaks that are uninformative; (2) there is no color change upon speciation change that could be characterized by UV-vis spectroscopy, and (3) electrospray ionization mass spectrom-

etry has limited utility since Nb has only one isotope and therefore lacks defining peak envelopes observed for V, Mo, and W POMs that have multiple isotopes.<sup>52</sup> Furthermore, we hypothesized that the larger species were observed in solution with larger alkalis because of more extensive linking of the  $\text{Nb}_{24}$  clusters by the alkalis. Finally, computational studies described a mechanism of conversion of  $\text{Nb}_{10}$  to  $\text{Nb}_{24}$  via an  $\text{Nb}_7$  intermediate, where the alkali cations bond to the most basic oxygens of  $\text{Nb}_{10}$ , initiating disassembly of the POM. This process exposes basic terminal oxygens that protonate, increasing the pH and increasing the reaction rate in unbuffered solutions (Figure 1).

This initial discovery of the reactivity of  $\text{Nb}_{10}$  promoted by alkalis in water was published without the benefit of a crystal structure for the absolute identification of  $\text{Nb}_{24}$ . We hypothesized that the gelation behavior was due to the lability of  $\text{Nb}_{24}$  in solution, especially the three  $\text{H}_2\text{O}---\text{Nb}=\text{O}$  that link the three  $\text{Nb}_7$  units in a ring. The terminal water presents an opportunity for further hydrolysis/condensation reactions that would lead to a gel-like network upon evaporation of the solvent. Additionally, ESI-MS (electrospray ionization mass spectroscopy) identified a cationic  $\text{Nb}_3$  fragment<sup>1</sup> that is the counterpart to the very reactive  $\text{Nb}_7$  fragment (Figure 1), which is not readily detected by SAXS in a solution dominated by much larger  $\text{Nb}_{24}$ . These small, oppositely charged units could also play a role in promoting network formation. As a first attempt to crystallize the  $\text{Nb}_{24}$  units in these reactions, we simply combined lithium uranyl triperoxide,  $\text{Li}_4\text{UO}_2(\text{O}_2)_3 \cdot n\text{H}_2\text{O}$ ,<sup>53</sup> with  $\text{Nb}_{10}$  in water. Uranyl with its trans-*yl*-oxo units could serve as a more stable substitute for the  $\text{H}_2\text{O}---\text{Nb}=\text{O}$  units in  $\text{Nb}_{24}$  (Figure 2B), while the Li both provides a counterion for crystallization and promotes the disassembly of  $\text{Nb}_{10}$ . Moreover, uranyl triperoxide is soluble in basic solutions. This strategy worked exactly as hoped, and two  $\text{Nb}_{24}$  assemblies substituted with the uranyl were crystallized (Figure 2C).<sup>47</sup> We also crystallized a dimer of the  $\text{Nb}_7$  unit. These were all obtained from the same reaction solution along with precipitated gels, demonstrating that (1) the  $\text{Nb}_{24}$  units are

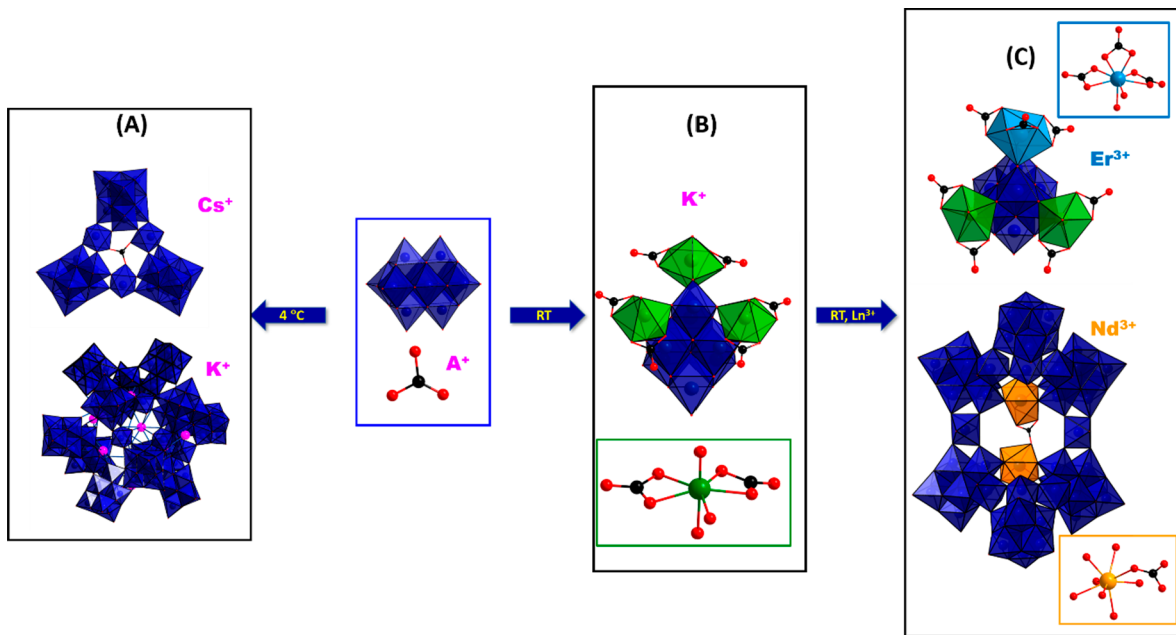


**Figure 4.** Reaction of  $\text{Nb}_{10}$  plus alkali carbonates leading to carbonate ligated Nb-POMs (blue box).<sup>3</sup> (A) Crystals grown at 4 °C with Cs-carbonate feature  $\text{Nb}_{24}-\text{CO}_3$  (top) and with K-carbonate feature  $\text{Nb}_{96}$  (bottom). (B) Room-temperature  $\text{Nb}_{10}$  plus K-carbonate yields  $\text{Nb}_{10}$ -carbonate. (C) Room-temperature reaction of  $\text{Nb}_{10}$  plus K-carbonate with added lanthanides yields  $\text{Er}-\text{Nb}_{24}\text{CO}_3$  (top) and  $\text{Nd}-\text{Nb}_{48}\text{CO}_3$  (bottom). Blue and green polyhedra are Nb, turquoise polyhedron and spheres are Er, and orange polyhedra and spheres are Nd. Red and black spheres are, respectively, oxygen and carbon.

quite labile and dynamic and (2) gelation remains the dominant behavior of these mixed species solutions.

#### Exploiting the Gelation Behavior of Aqueous $\text{Nb}_{10}$

In the course of solution studies with  $\text{Nb}_{10}$ , we recognized that (1) virtually any water-soluble ion, even sparingly soluble ions, would invoke the evolution of  $\text{Nb}_{10}$  to  $\text{Nb}_{24}$  (Figure 3A) and (2)  $\text{Nb}_{24}$  solutions exhibited higher solubility than  $\text{Nb}_{10}$  solutions, even in the presence of the added electrolytes (i.e., alkalis plus counteranions). We decided that this behavior could be ideally exploited in the deposition of niobate thin films. One of the most industrially important niobate materials is perovskite ( $\text{K}_x\text{Na}_y\text{NbO}_3$  (KNN), used as a lead-free piezoelectric in microelectronics. Aqueous deposition processes are desirable, and the state-of-the-art aqueous solution deposition of KNN utilizes 0.25 molar ammonium niobium oxalate with  $\text{K}^+$  and  $\text{Na}^+$  nitrates,<sup>54</sup> where nitrates are not desirable for industrial processes. Moreover, the relatively low concentration of Nb means thick film applications (i.e., actuators) require multiple deposition steps. Using  $\text{Nb}_{24}$  solutions, we demonstrated the deposition of KNN from solutions with 1 M Nb, near neutral pH, and no nitrate.<sup>55</sup> In these solutions, Na and K are added as carbonate salts for two reasons: (1) the carbonate is readily removed during the annealing process and (2) carbonate increases the basicity of these solutions, enabling more rapid  $\text{Nb}_{10}$  to  $\text{Nb}_{24}$  conversion. Carbonate also proved to be an excellent ligand for the crystallization of several new members of the family of  $\text{Nb}_{10}$  disassembly–reasembly reaction products (discussed later). To compare the deposition of  $\text{Nb}_2\text{O}_5$  from  $\text{Nb}_{10}$  and  $\text{Nb}_{24}$ , we prepared up to 2.5 molar  $\text{Nb}_{10}$  with added ammonium nitrate ( $\text{NH}_4-\text{Nb}_{24}$ ) and deposited films by spin-coating followed by annealing. Flat and smooth films were obtained from 2.5 M Nb (as predominantly  $\text{Nb}_{24}$ ), whereas all concentrations of  $\text{Nb}_{10}$  (i.e., >0.5 M) yielded rough and nonconformal films (Figure

3B,C).<sup>55</sup> We attribute this to the gelation behavior of  $\text{Nb}_{24}$  vs the crystallization behavior of  $\text{Nb}_{10}$ .

Next, we demonstrated that one could essentially contact a  $\text{Nb}_{10}$  solution with sparingly soluble phases (including  $\text{Ca}(\text{OH})_2$ ,  $\text{Ag}_2\text{CO}_3$ , and  $\text{CuCO}_3$ ) to promote the  $\text{Nb}_{10}$  to  $\text{Nb}_{24}$  conversion. Contacting these with  $\text{Nb}_{10}$  solutions (2.5 M Nb) increased the pH from neutral to ~9, and a few percent of these metals was doped into the deposited  $\text{Nb}_2\text{O}_5$  films, evidencing their slight dissolution. SAXS of these solutions showed an impressive “structure factor”, in addition to features indicative of  $\text{Nb}_{24}$  clusters in solution (Figure 3D).<sup>1,55</sup> The structure factor, also called a Coulombic peak, indicates the ordering of clusters in solution, and the position of the peak on the  $q$  scale ( $\text{\AA}^{-1}$ ) provides the average distance between clusters. This phenomenon is also described as “repulsion” between same-charge species, and in fact it can be diminished by adding shielding electrolytes. This prominent feature is consistent with solutions that are highly concentrated, with highly charged species (i.e.,  $[\text{H}_x\text{Nb}_{24}\text{O}_{72}]^{(24-x)-}$ ) and minimal shielding electrolytes.

#### Additional Structures Featuring the $\text{Nb}_7/\text{Nb}_{24}$ Unit from $\text{Nb}_{10}$ to $\text{Nb}_{24}$ Conversion: From $\text{Nb}_{10}$ -Alkali Carbonate (and Lanthanide) Solutions

As mentioned above, the addition of alkali carbonates to  $\text{Nb}_{10}$  solutions was an effective means to form highly soluble  $\text{Nb}_{24}$  solutions that are tailored for the deposition of niobate thin films. Under the right conditions, carbonate also proved to be a useful ligand for Nb to obtain diverse topologies. From a Cs carbonate– $\text{Nb}_{10}$  solution at 4 °C, we obtained  $\text{Nb}_{24}-\text{CO}_3$ , with a single carbonate anion replacing the three terminal  $\text{H}_2\text{O}$  of the  $\text{H}_2\text{O}-\text{Nb}=\text{O}$  unit that is highlighted in Figure 2B ( $[\text{Nb}_{24}\text{O}_{69}(\text{CO}_3)]^{20-}$ , Figure 4A).<sup>3</sup> From K carbonate– $\text{Nb}_{10}$  solution at 4 °C, we obtained  $\text{K}-\text{Nb}_{96}$  (Figure 4A, tetrahedral arrangement of four  $\text{Nb}_{24}$  linked by  $\text{K}^+$ , prior published by

Huang<sup>56</sup>). Leaving these crystals in contact with the mother liquor at room temperature leads to transformation to a different Nb<sub>10</sub> arrangement that features carbonate ligands as well as the Nb<sub>7</sub> unit (Figure 4B).<sup>3</sup> The “naked” Nb<sub>7</sub> (Figure 1) has three terminal cis-oxo ligands, clearly an unstable configuration for Nb<sup>5+</sup>, and a point of linking (or gelling, both a product of hydrolysis/condensation reactions), ultimately leading to larger assemblies such as Nb<sub>24</sub>. In fact, while cis-yl-oxos are recognized in Mo-POM chemistry (i.e.,  $\alpha$ -[Mo<sub>8</sub>O<sub>26</sub>]<sup>4-</sup>), they are largely unknown for Nb-POM chemistry, attributed to Nb’s lower charge and concomitant inability to form two Nb=O. In Nb<sub>10</sub>-CO<sub>3</sub> (formulated as [Nb<sub>10</sub>O<sub>25</sub>(CO<sub>3</sub>)<sub>6</sub>]<sup>12-</sup>, Figure 4B), the aforementioned three cis terminal oxos of the Nb<sub>7</sub> unit bridge three additional Nb polyhedra, and each one is pentagonal bipyramidal with two chelating carbonate ligands in the pentagonal plane (Figure 4B). Nb<sub>10</sub>-carbonate was crystallized in two frameworks, with one featuring a K<sup>+</sup>-linked dimer, [Nb<sub>10</sub>-CO<sub>3</sub>]<sub>2</sub>, that surprisingly is retained upon redissolution in water.<sup>3</sup> This is yet another example of how important the alkalis are for highly charged Nb-POMs in both speciation and supramolecular assembly. In this same study, we also added lanthanides to the Nb<sub>10</sub>-K<sub>2</sub>CO<sub>3</sub> aqueous solutions and obtained two Ln-substituted clusters (Figure 4C). In the first structure, termed Er-Nb<sub>9</sub>CO<sub>3</sub> ([Nb<sub>9</sub>ErO<sub>24</sub>(CO<sub>3</sub>)<sub>7</sub>]<sup>14-</sup>, Figure 4C), Er<sup>3+</sup> replaces Nb=O<sup>3+</sup> for one of the carbonate-ligated Nb-polyhedra, and it has three chelating carbonate ligands instead of two. The second Ln-substituted Nb-POM, denoted Nd-Nb<sub>48</sub>CO<sub>3</sub>, [(Nd<sub>2</sub>O<sub>5</sub>(Nb<sub>7</sub>O<sub>22</sub>)<sub>6</sub>(CO<sub>3</sub>)(NbO(H<sub>2</sub>O))<sub>6</sub>]<sup>42-</sup>, Figure 4C] can be described as two NdNb<sub>23</sub> rings, with a Nd<sup>3+</sup> replacing one of the three bridging [H<sub>2</sub>O--Nb=O]<sup>3+</sup> units within a typical Nb<sub>24</sub> ring. Recently, the group of S. T. Zheng reported a very similar Dy<sup>3+</sup> substitution of [H<sub>2</sub>O--Nb=O]<sup>3+</sup> within the Nb<sub>24</sub> units, building fantastic Nb-Dy frameworks.<sup>42,57,58</sup> With the modification of this family, Zheng identified the first evidence for reduced Nb within an Nb-POM.<sup>58</sup> Notably these were obtained by more typical Nb-POM syntheses that involve hexaniobate starting materials, hydrothermal processing, and several other reagents including Cu-ethylenediamine cations, oxalate, and triazole, where Cu and oxalate are included in the crystallized lattices. On the other hand, the goal of developing syntheses based on Nb<sub>10</sub> is simple approaches wherein reaction pathways can be explained and predicted. Ultimately, we hope to mirror the control that can be executed in W-POM and Mo-POM chemistries, predominantly via pH in these systems and counterions in Nb-POM systems.

#### New Nb-POMs from Nb<sub>10</sub> Plus Poorly Soluble Transition-Metal Carbonates

We have crystallized and structurally characterized two additional Nb<sub>24</sub>-based cluster assemblies from the above approach of contacting aqueous Nb<sub>10</sub> solutions with sparingly soluble metal oxides/carbonates, exploited in thin film deposition. These are reported here for the first time, and additional information concerning synthesis, characterization, and crystallographic data (Table S1) is available in the SI.

**Ag<sub>3</sub>Nb<sub>48</sub>.** From the Ag<sub>2</sub>CO<sub>3</sub>-Nb<sub>10</sub> experiment, we obtained Ag<sub>3</sub>Nb<sub>48</sub> (Figure 5A), charge-balanced by K<sup>+</sup> and TMA<sup>+</sup> (21 and 15, respectively, Table S2). Potassium chloride was added to aid crystallization. Since this is the first report of Ag<sub>3</sub>Nb<sub>48</sub>, we describe its structure in a little more detail. Based on BVS calculations (bond valence sum, Figure S1 and Table S3), the Nb-POM is formulated

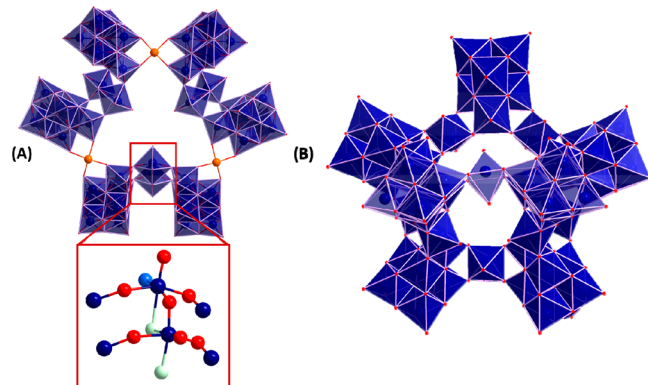


**Figure 5.** (A) Ag<sub>3</sub>Nb<sub>48</sub> full cluster (top). Bottom inset shows the dimer unit. Turquoise spheres are a terminal hydroxide, sea green spheres are water molecules, and the remainder (red) are oxos. Blue spheres and polyhedra are Nb, and orange spheres are Ag. (B) Nb<sub>59</sub>, blue polyhedra are Nb. Nb<sub>59</sub> has no symmetry elements, only a pseudomirror plane bisecting Nb<sub>59</sub> vertically in this current view.

[Ag<sub>3</sub>Nb<sub>48</sub>O<sub>138</sub>(OH)<sub>3</sub>(H<sub>2</sub>O)<sub>6</sub>]<sup>36-</sup>. The Ag<sub>3</sub>Nb<sub>48</sub> ring has C<sub>3v</sub> symmetry, composed of six Nb<sub>7</sub> units in three sets; each set is bridged by an [Nb<sub>2</sub>O<sub>4</sub>(OH)(H<sub>2</sub>O)<sub>2</sub>]<sup>+</sup> dimer (Figure 5A, bottom). This dimer has some unprecedented features in Nb-POM chemistry. Namely, one Nb=O in the dimer unit is cis to a terminal hydroxide; neither cis-terminal ligands nor terminal hydroxides are generally observed in Nb-POMs (as mentioned above). The second Nb=O ligand is trans to a water ligand, as typically found in the Nb<sub>24</sub> ring. Finally, the Nb-dimer unit is quite asymmetric, bridged by an oxo ligand and a water ligand, and the bridging water ligand is also unprecedented. See Figure S1 and Table S3 for more details and BVS assignment of oxo/hydroxyl/water. The three Nb<sub>7</sub>-Nb<sub>2</sub>-Nb<sub>7</sub> subunits are linked into a ring by three square planar Ag, two bonds bridging Nb=O of the core Nb<sub>6</sub> unit, and two bonds to the addenda seventh Nb of the Nb<sub>7</sub> unit. (Ag–O = 2.062(7) and 1.947(7) Å, respectively). The Ag<sub>3</sub>Nb<sub>48</sub> are linked together in offset layers in the ab plane by K cations (Figure S2).

**Nb<sub>59</sub>.** Nb<sub>59</sub>, formulated as [(Nb<sub>59</sub>O<sub>164</sub>)(H<sub>2</sub>O)<sub>10</sub>]<sup>33-</sup>, was obtained from the contact of Nb<sub>10</sub> solution with manganese carbonate followed by the addition of KCl for crystallization; details are provided in the SI. While K<sup>+</sup> is found in the lattice as counterions (12 total, the remainder of counterions for charge balance are presumed to be TMA, see Table S2), manganese is not located in the lattice. Clearly, the only role of manganese carbonate is in promoting the disassembly of Nb<sub>10</sub>-Nb<sub>59</sub> is structurally fascinating because it has no rigorous symmetry elements that define its topology, only a pseudo mirror plane (Figure 5B). This representative structure from aqueous Nb<sub>24</sub>-type solutions suggests yet another contributing factor to the poor crystallization behavior of these solutions. Nb<sub>59</sub> is built of Nb<sub>7</sub> units linked by H<sub>2</sub>O--Nb=O monomers in rings, similar to Nb<sub>24</sub>. It consists of a ring of five Nb<sub>7</sub>, alternating with five monomers, where the seventh addenda Nb-octahedron of the Nb<sub>7</sub> unit bridges to two monomers within the ring. Four of the Nb<sub>7</sub> units further bridge an additional monomer approximately perpendicular to the pentagonal ring, and these four link an Nb<sub>7</sub>-monomer-Nb<sub>7</sub> bridge, resembling a handle of a pentagon-shaped basket. The pseudo mirror plane is perpendicular to the pentagonal ring and bisects the “handle”.

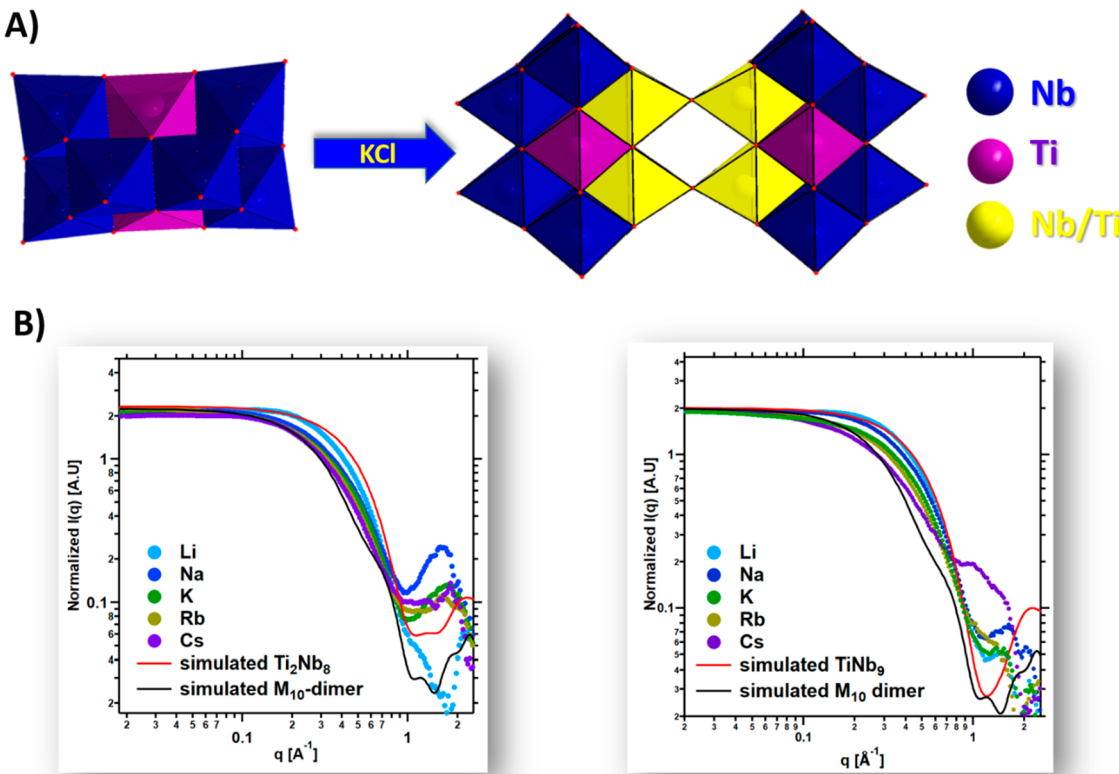


**Figure 6.** (A, Left)  $[\text{Ti}_2\text{Nb}_8\text{O}_{28}]^{8-}$  representing a typical disubstituted decametalate, where heterometals substitute in the octahedra that do not have terminal oxo-ligands (purple polyhedra).  $\text{Ti}_2\text{Nb}_8$  dissolved with KCl crystallizes  $[\text{Ti}_6\text{Nb}_{14}\text{O}_{54}]^{14-}$  (right). Further substitution of Ti (50%) in the yellow polyhedra and dimerization indicate disassembly–reassembling reactions. (B) SAXS of  $\text{Ti}_2\text{Nb}_8$  (left) and  $\text{TiNb}_9$  (right) with added alkalis. Also included in both plots are the simulated scattering for the  $\text{M}_{10}$  cluster and the  $\text{M}_{10}$  dimer (clusters shown in part A). The Guinier region of the experimental curves falls between these two simulated curves, suggesting partial dimerization of the decametalates, and there appears to be increasing dimerization with increased alkali size, similar to the reactivity of  $\text{Nb}_{10}$ . Because the shift of the Guinier curve is not as dramatic as the  $\text{Nb}_{10} \rightarrow \text{Nb}_{24}$  transformation (i.e., Figure 2A) and the scattering curves are missing the characteristic plateau at  $q \approx 0.6 \text{ Å}^{-1}$  (i.e., Figure 3D), we are confident that  $\text{Nb}_{24}$  is not a dominant species in these solutions, different from the reactivity of  $\text{Nb}_{10}$  (adapted with permission from ref 71 copyright (2022), Wiley-VCH Verlag GmbH&Co. KGaA).

### Transition-Metal-Substituted Decametalates

The decaniobate topology is readily substituted with other transition metals that do not form a stable  $M=O$  terminal oxo bond since  $\text{M}_{10}$  contains two octahedral sites where all oxos are bridging (Figure 6A). Decavanadate also exhibits some substitution chemistry, i.e., substitution of Pt,<sup>59</sup> Te,<sup>60</sup> and Mo.<sup>61</sup> Surprisingly, more substituted decametalate compositions have been reported for niobate (Ti, Fe, Cr, Ni, Mn, and Co)<sup>62–65</sup> than for vanadate, perhaps due to the relative lability of the niobate, in contrast to the high stability of the vanadate. In addition, a similar structure that resembles two fused Lindqvist ions,  $[\text{Cr}_2(\text{OH})_4\text{Nb}_{10}\text{O}_{30}]^{8-}$ , was also isolated.<sup>64</sup> The aforementioned open-shell transition-metal substitutions in decaniobate (and similar structures) were accomplished by the use of only TMA counterions, which enables the solubility of these metals under alkaline conditions (plus very precise workup of the crude product).<sup>66,67</sup> The first heterometal substitution in  $\text{Nb}_{10}$  was not an open-shell transition metal or isolated as a TMA salt. Specifically,  $[\text{Ti}_2\text{Nb}_8\text{O}_{28}]^{8-}$  was isolated as a Na salt,<sup>65</sup> obtained from exploratory hydrothermal synthesis in the early days of Nb-POM development. This was a relatively straightforward synthesis and not surprising because (1) Ti is a transition metal that exhibits rare base solubility and (2)  $\text{Ti}^{4+}$  and  $\text{Nb}^{5+}$  have nearly identical octahedral coordination radii. Following this, Villa synthesized the monosubstituted and disubstituted decametalate ( $\text{TiNb}_9$

and  $\text{Ti}_2\text{Nb}_8$ ) as tetramethylammonium (TMA) salts and studied their oxo-ligand lability in water.<sup>68</sup> They noted increasing stability at higher pH with increasing cluster charge (i.e., stability trends  $\text{Nb}_{10}^{6-} < \text{TiNb}_9^{7-} < \text{Ti}_2\text{Nb}_8^{8-}$ ). We also studied the lability of  $\text{TiNb}_9$  and  $\text{Ti}_2\text{Nb}_8$ , promoted by interactions with alkalis, hypothesizing that they may also exhibit disassembly–reassembling activity.<sup>69</sup> TMA salts of  $\text{TiNb}_9$  and  $\text{Ti}_2\text{Nb}_8$  combined with alkali chlorides studied by SAXS (Figure 6B) indicated the growth of larger species but different from  $\text{Nb}_{24}$ . A crystal structure of a minor phase explained the SAXS and revealed that disassembly–reassembling of the Ti-substituted decaniobate also occurs. A  $\text{Ti}_3\text{Nb}_7$  dimer, formulated as  $[\text{Ti}_6\text{Nb}_{14}\text{O}_{54}]^{14-}$ , was crystallized (Figure 6A) from a solution of KCl plus  $\text{Ti}_2\text{Nb}_8$ . This type of dimerization of  $\text{Nb}_{10}$  to  $\text{Nb}_{20}$  was observed in 2006<sup>70</sup> in organic media. Furthermore, Villa<sup>50</sup> identified the terminal oxos that are the point of dimerization as the most labile oxygens in the cluster,<sup>50</sup> explaining this dimerization. However, what is more surprising is that there is additional substitution of Ti into the polyhedra that link the two decametalate units (50% Ti, 50% Nb occupancy; see Figure 6A), which is evidence for the partial disassembly of  $\text{Ti}_2\text{Nb}_8$ , aside from the lability of the terminal oxos that leads to dimerization. It is possible that more aggressive reaction conditions could lead to TM-substituted  $\text{Nb}_{24}$  derivatives, with the transient formation of  $\text{M}_7$  units ( $\text{M} = \text{Nb}, \text{TM}$ ).

Reported here for the first time, the reactivity of Nb<sub>10</sub> with poorly soluble copper carbonate, followed by crystallization with K<sup>+</sup>, led to the crystallization of H<sub>4</sub>K<sub>8</sub>[Cu<sub>2</sub>Nb<sub>8</sub>O<sub>28</sub>]·11H<sub>2</sub>O. Substitution of Cu(II) into the decametalate structure, tetra-protonation of this topology, and disubstitution of an open-shell transition metal was not observed previously.<sup>63</sup> However, this is a minor product, and all prior-isolated analogues were crystallized with TMA. BVS and rationalization of the assigned structure/formula are included in the SI. Solution-phase characterization, SAXS, and Raman spectroscopy (Figures S5–S8, Table S5) indicate that Nb<sub>24</sub> is the major reaction product upon contacting sparingly soluble CuCO<sub>3</sub> with Nb<sub>10</sub> solution, similar to the solutions from which Ag<sub>3</sub>Nb<sub>48</sub> and Nb<sub>59</sub> were obtained (Figure S5). However, it is easy to imagine how Nb<sub>7</sub> subunits can reform the decametalate, the driving force being stabilization of the substituted transition metal, as observed previously in Casey's studies of Ti-substituted decaniobate.<sup>68</sup>

## SUMMARY AND OUTLOOK

Our strategy of Nb<sub>10</sub> disassembly–reassembly in mild-pH and room-temperature solutions has not only led to new Nb-POM topologies but has also brought forth a more in-depth understanding of Nb-speciation, recently summarized in computed speciation diagrams.<sup>72</sup> This work has also shed light on the possible roles of alkalis in aqueous reactions, aside from templating or dictating solubility. This knowledge and insight goes beyond POM chemistry and toward inorganic and organic synthesis, solubility in complex media, and contaminant transport in natural settings. A challenge that still remains with Nb-POM chemistry that may never be overcome is the inability to controllably synthesize heterometal-functionalized Nb-POMs (metals include open-shell transition metals and f-elements) with metals that largely exhibit poor solubility under neutral to alkaline conditions. Yet these heterometals impart interesting properties such as magnetism, luminescence, and photochemical and electrochemical responses. It is true that hybrid POMs and materials have been synthesized with Nb-POMs and these acid-soluble metals, including those reviewed and reported here. However, these rarely can be made pure without the coprecipitation of insoluble hydroxides of the heterometal. It is likely that ionic liquids, polymer solutions, or other innovative solvent mixtures will be required. This also represents a broader impact in creating robust, task-specific liquids. The high solubility derived from the Nb<sub>10</sub> → Nb<sub>24</sub> transformation is surprising, as is the gelation behavior of such solutions. We intend to continue exploiting this gelation behavior, targeting glassy hybrid (metal–organic) materials and porous solids with functions such as base catalysis and CO<sub>2</sub> capture.

## ASSOCIATED CONTENT

### Supporting Information

The Supporting Information is available free of charge at <https://pubs.acs.org/doi/10.1021/acs.accounts.3c00583>.

Experimental section and characterization (PDF)

### Accession Codes

CCDC 2291413–2291415 contain the supplementary crystallographic data for this paper. These data can be obtained free of charge via [www.ccdc.cam.ac.uk/data\\_request/cif](http://www.ccdc.cam.ac.uk/data_request/cif), or by emailing [data\\_request@ccdc.cam.ac.uk](mailto:data_request@ccdc.cam.ac.uk), or by contacting The

Cambridge Crystallographic Data Centre, 12 Union Road, Cambridge CB2 1EZ, UK; fax: +44 1223 336033.

## AUTHOR INFORMATION

### Corresponding Author

**May Nyman** — Department of Chemistry, Oregon State University, Corvallis, Oregon 97331, United States;  
✉ [orcid.org/0000-0002-1787-0518](https://orcid.org/0000-0002-1787-0518); Email: [may.nyman@oregonstate.edu](mailto:may.nyman@oregonstate.edu)

### Authors

**Tasnim Rahman** — Department of Chemistry, Oregon State University, Corvallis, Oregon 97331, United States

**Ian Colliard** — Department of Chemistry, Oregon State University, Corvallis, Oregon 97331, United States;  
✉ [orcid.org/0000-0003-1883-1155](https://orcid.org/0000-0003-1883-1155)

Complete contact information is available at:  
<https://pubs.acs.org/10.1021/acs.accounts.3c00583>

### Author Contributions

CRediT: **May Nyman** project administration, resources, supervision, writing-original draft, writing-review & editing; **Tasnim Rahman** investigation, writing-review & editing; **Ian Colliard** formal analysis, investigation.

### Notes

The authors declare no competing financial interest.

### Biographies

**May Nyman** has been a professor of chemistry at Oregon State University since 2012. From 1998 to 2012, she was a staff scientist at Sandia National Laboratories in Albuquerque, New Mexico. May has a Ph.D. in chemistry, an M.Sc. in materials science and engineering, and a B.Sc. in geology. May's research group studies aqueous inorganic molecules for critical material separations, nuclear fuel cycle separations, carbon capture, and a fundamental understanding of self-assembly, supramolecular assembly, and crystallization.

**Tasnim Rahman** is currently a postdoctoral researcher at Argonne National Laboratory. Tasnim obtained her doctorate in materials chemistry in 2022 under the mentorship of May Nyman at Oregon State University. Tasnim's Ph.D. research involved understanding polyoxoniobate speciation, chemical and structural behavior in solution, and applications. At Argonne, Tasnim is currently using SAXS to study solvent extraction of rare earth elements.

**Ian Colliard** is currently a postdoctoral researcher at Lawrence Livermore National Laboratory. Ian obtained his doctorate in materials chemistry in 2022 under the mentorship of May Nyman at Oregon State University. At OSU, Ian found his “superpower” in the crystallization of metal-oxo clusters and exploring the mysteries therein, first and foremost, from crystallography.

## ACKNOWLEDGMENTS

The development of much of the content of this Account and original research herein was supported by the U.S. Department of Energy, Office of Basic Energy Sciences, Division of Material Sciences and Engineering under award DE SC0010802. MN thanks Companhia Brasileira de Metalurgia e Mineração, (CBMM) for multiple generous gifts of hydrous niobium oxide, enabling 2 decades of Nb-POM research.

## ■ REFERENCES

- (1) Sures, D.; Segado, M.; Bo, C.; Nyman, M. Alkali-Driven Disassembly and Reassembly of Molecular Niobium Oxide in Water. *J. Am. Chem. Soc.* **2018**, *140* (34), 10803–10813.
- (2) Rahman, T.; Martin, N. P.; Jenkins, J. K.; Elzein, R.; Fast, D. B.; Addou, R.; Herman, G. S.; Nyman, M.  $\text{Nb}_2\text{O}_5$ ,  $\text{LiNbO}_3$ , and  $(\text{Na}, \text{K})\text{NbO}_3$  Thin Films from High-Concentration Aqueous Nb-Polyoxometalates. *Inorg. Chem.* **2022**, *61* (8), 3586–3597.
- (3) Amiri, M.; Martin, N. P.; Feng, C. L.; Lovio, J. K.; Nyman, M. Deliberate Construction of Polyoxoniobates Exploiting the Carbonate Ligand. *Angew. Chem. Int. Edit* **2021**, *60* (22), 12461–12466.
- (4) Bagai, R.; Christou, G. The Drosophila of Single-Molecule Magnetism:  $[\text{Mn}_{12}\text{O}_{12}(\text{O}_2\text{CR})_{16}(\text{H}_2\text{O})_4]$ . *Chem. Soc. Rev.* **2009**, *38* (4), 1011–1026.
- (5) Nyman, M. Polyoxoniobate Chemistry in the 21st Century. *Dalton Transac* **2011**, *40* (32), 8049–8058.
- (6) Nyman, M.; Bonhomme, F.; Alam, T. M.; Rodriguez, M. A.; Cherry, B. R.; Krumhansl, J. L.; Nenoff, T. M.; Sattler, A. M. A General Synthetic Procedure for Heteropolyniobates. *Science* **2002**, *297* (5583), 996–998.
- (7) Liu, Z. Y.; Lin, Y. D.; Yu, H.; Chen, H. N.; Guo, Z. W.; Li, X. X.; Zheng, S. T. Recent Advances in Polyoxoniobate-Catalyzed Reactions. *Tungsten-Switzerland* **2022**, *4* (2), 81–98.
- (8) Wu, Y. L.; Li, X. X.; Qi, Y. J.; Yu, H.; Jin, L.; Zheng, S. T.  $\{\text{Nb}_{288}\text{O}_{768}(\text{OH})_{48}(\text{CO}_3)_{12}\}$ : A Macromolecular Polyoxometalate with Close to 300 Niobium Atoms. *Angew. Chem. Int. Edit* **2018**, *57* (28), 8572–8576.
- (9) Tian, Y. Y.; Kaledin, A. L.; Collins-Wildman, D. L.; Snider, V. G.; Musaev, D. G.; Hill, C. L.; Frenkel, A. I. Polyniobate Nanothreads for Decomposition of the Nerve Agent Simulant Dimethyl Chlorophosphate. *Acs Appl. Nano Mater.* **2021**, *4* (6), 5649–5654.
- (10) Casey, W. H.; Rustad, J. R.; Spiccia, L. Minerals as Molecules—Use of Aqueous Oxide and Hydroxide Clusters to Understand Geochemical Reactions. *Chem.—Eur. J.* **2009**, *15* (18), 4496–4515.
- (11) Kondinski, A.; Parac-Vogt, T. N. Keggin Structure, Quo Vadis? *Front Chem.* **2018**, *6*, DOI: 10.3389/fchem.2018.00346.
- (12) Gumerova, N. I.; Rompel, A. Polyoxometalates in Solution: Speciation under Spotlight. *Chem. Soc. Rev.* **2020**, *49* (21), 7568–7601.
- (13) Gumerova, N. I.; Rompel, A. Synthesis, Structures and Applications of Electron-Rich Polyoxometalates. *Nat. Rev. Chem.* **2018**, *2* (2), DOI: 10.1038/s41570-018-0112.
- (14) Streb, C. Structure and Bonding in Molecular Vanadium Oxides: From Templates Via Host-Guest Chemistry to Applications. *Struct. Bonding (Berlin)* **2017**, *176*, 31–47.
- (15) Muller, A.; Roy, S. En Route from the Mystery of Molybdenum Blue Via Related Manipulatable Building Blocks to Aspects of Materials Science. *Coordin Chem. Rev.* **2003**, *245* (1–2), 153–166.
- (16) Nyman, M.; Burns, P. C. A Comprehensive Comparison of Transition-Metal and Actinyl Polyoxometalates. *Chem. Soc. Rev.* **2012**, *41* (22), 7354–7367.
- (17) Goiffon, A.; Philippot, E.; Maurin, M. Structure Cristalline Du Niobate 7/6 De Sodium  $(\text{Na}_7)(\text{H}_3\text{O})\text{Nb}_6\text{O}_{19}$  14  $\text{H}_2\text{O}$ . *Revue de Chimie Minerale* **1980**, *17*, 466–476.
- (18) Balogh, E.; Anderson, T. M.; Rustad, J. R.; Nyman, M.; Casey, W. H. Rates of Oxygen-Isotope Exchange between Sites in the  $[\text{H}_x\text{Ta}_6\text{O}_{19}]^{(8-x)-}$  (aq) Lindqvist Ion and Aqueous Solutions: Comparisons to  $[\text{H}_x\text{Nb}_6\text{O}_{19}]^{(8-x)-}$  (aq). *Inorg. Chem.* **2007**, *46* (17), 7032–7039.
- (19) Nyman, M.; Alam, T. M.; Bonhomme, F.; Rodriguez, M. A.; Frazer, C. S.; Welk, M. E. Solid-State Structures and Solution Behavior of Alkali Salts of the  $[\text{Nb}_6\text{O}_{19}]^{8-}$  Lindqvist Ion. *J. Clust Sci.* **2006**, *17* (2), 197–219.
- (20) Fullmer, L. B.; Mansergh, R. H.; Zakharov, L. N.; Keszler, D. A.; Nyman, M.  $\text{Nb}_2\text{O}_5$  and  $\text{Ta}_2\text{O}_5$  Thin Films from Polyoxometalate Precursors: A Single Proton Makes a Difference. *Cryst. Growth Des* **2015**, *15* (8), 3885–3892.
- (21) Fullmer, L. B.; Molina, P. I.; Antonio, M. R.; Nyman, M. Contrasting Ion-Association Behaviour of Ta and Nb Polyoxometalates. *Dalton T* **2014**, *43* (41), 15295–15299.
- (22) Filowitz, M.; Ho, R. K. C.; Klemperer, W. G.; Shum, W. O-17 Nuclear Magnetic-Resonance Spectroscopy of Polyoxometalates. 1. Sensitivity and Resolution. *Inorg. Chem.* **1979**, *18* (1), 93–103.
- (23) Song, Q.; Heng, S. L.; Wang, W. B.; Guo, H. L.; Li, H. Y.; Dang, D. B. Binary Type-II Heterojunction  $\text{K}_x\text{Nb}_6\text{O}_{19}/g\text{-C}_3\text{N}_4$ : An Effective Photocatalyst for Hydrogen Evolution without a Co-Catalyst. *Nanomaterials-Basel* **2022**, *12* (5), DOI: 10.3390/nano12050849.
- (24) Anderson, T. M.; Rodriguez, M. A.; Bonhomme, F.; Bixler, J. N.; Alama, T. M.; Nyman, M. An Aqueous Route to  $[\text{Ta}_6\text{O}_{19}]^{8-}$  and Solid-State Studies of Isostructural Niobium and Tantalum Oxide Complexes. *Dalton Transac* **2007**, No. 40, 4517–4522.
- (25) Nyman, M.; Anderson, T. M.; Provencio, P. P. Comparison of Aqueous and Non-Aqueous Soft-Chemical Syntheses of Lithium Niobate and Lithium Tantalate Powders. *Cryst. Growth Des* **2009**, *9* (2), 1036–1040.
- (26) Hou, Y.; Fast, D. B.; Ruther, R. E.; Amador, J. M.; Fullmer, L. B.; Decker, S. R.; Zakharov, L. N.; Dolgos, M. R.; Nyman, M. The Atomic Level Journey from Aqueous Polyoxometalate to Metal Oxide. *J. Solid State Chem.* **2015**, *221*, 418–425.
- (27) Antonio, M. R.; Nyman, M.; Anderson, T. M. Direct Observation of Contact Ion-Pair Formation in Aqueous Solution. *Angew. Chem. Int. Edit* **2009**, *48* (33), 6136–6140.
- (28) Hill, C. L. Introduction: Polyoxometalates - Multicomponent Molecular Vehicles to Probe Fundamental Issues and Practical Problems. *Chem. Rev.* **1998**, *98* (1), 1–2.
- (29) Zhao, Y.; Gao, D.; Liu, S.; Biskupek, J.; Kaiser, U.; Liu, R.; Streb, C. Pom@Zif Derived Mixed Metal Oxide Catalysts for Sustained Electrocatalytic Oxygen Evolution. *Chem.—Eur. J.* **2023**, e202203220.
- (30) Jordan, J. W.; Townsend, W. J. V.; Johnson, L. R.; Walsh, D. A.; Newton, G. N.; Khlobystov, A. N. Electrochemistry of Redox-Active Molecules Confined within Narrow Carbon Nanotubes. *Chem. Soc. Rev.* **2021**, *50* (19), 10895–10916.
- (31) Chen, J. J.; Vila-Nadal, L.; Sole-Daura, A.; Chisholm, G.; Minato, T.; Busche, C.; Zhao, T. T.; Kandasamy, B.; Ganin, A. Y.; Smith, R. M.; Colliard, I.; Carbó, J. J.; Poblet, J. M.; Nyman, M.; Cronin, L. Effective Storage of Electrons in Water by the Formation of Highly Reduced Polyoxometalate Clusters. *J. Am. Chem. Soc.* **2022**, *144* (20), 8951–8960.
- (32) Anjass, M.; Lowe, G. A.; Streb, C. Molecular Vanadium Oxides for Energy Conversion and Energy Storage: Current Trends and Emerging Opportunities. *Angew. Chem. Int. Edit* **2021**, *60* (14), 7522–7532.
- (33) Schreiber, E.; Garwick, R. E.; Baran, M. J.; Baird, M. A.; Helms, B. A.; Matson, E. M. Molecular Engineering of Polyoxovanadate-Alkoxide Clusters and Microporous Polymer Membranes to Prevent Crossover in Redox-Flow Batteries. *Acs Appl. Mater. Inter* **2022**, *14* (20), 22965–22972.
- (34) Aureliano, M.; Mitchell, S. G.; Yin, P. C. Editorial: Emerging Polyoxometalates with Biological, Biomedical, and Health Applications. *Front Chem.* **2022**, *10*, DOI: 10.3389/fchem.2022.977317.
- (35) Kim, G. S.; Zeng, H. D.; VanDerveer, D.; Hill, C. L. A Supramolecular Tetra-Keggin Polyoxometalate  $[\text{Nb}_4\text{O}_6(\text{Alpha}-\text{Nb}_3\text{SiW}_9\text{O}_{40})_4]^{20-}$ . *Angew. Chem. Int. Edit* **1999**, *38* (21), 3205–3207.
- (36) Kim, G. S.; Zeng, H. D.; Rhule, J. T.; Weinstock, I. A.; Hill, C. L. Synthesis, X-Ray Structure, and Hydrolytic Chemistry of the Highly Potent Antiviral Polyniobutungstate a-Alpha-[ $\text{Si}_2\text{Nb}_3\text{W}_{18}\text{O}_{77}$ ] $^{8-}$ . *Chem. Commun.* **1999**, No. 17, 1651–1652.
- (37) Weiner, H.; Aiken, J. D.; Finke, R. G. Polyoxometalate Catalyst Precursors. Improved Synthesis, H<sup>+</sup>-Titration Procedure, and Evidence for P-31 NMR as a Highly Sensitive Support-Site Indicator for the Prototype Polyoxoanion-Organometallic-Support System  $[(\text{Eta}-\text{C}_4\text{H}_9)_4\text{N}]_9\text{P}_2\text{W}_{15}\text{Nb}_3\text{O}_{62}$ . *Inorg. Chem.* **1996**, *35* (26), 7905–7913.

- (38) Flynn, C. M.; Stucky, G. D. Crystal Structure of Sodium 12-Niobomanganate(IV)  $\text{Na}_{12}\text{MnNb}_{12}\text{O}_{38}\cdot5\text{H}_2\text{O}$ . *Inorg. Chem.* **1969**, *8* (2), 335–344.
- (39) Besserguenev, A. V.; Dickman, M. H.; Pope, M. T. Robust, Alkali-Stable, Triscarbonyl Metal Derivatives of Hexametalate Anions,  $[\text{M}_6\text{O}_{19}\{\text{M}'(\text{CO})_3\}_n]^{(8-n)^-}$  ( $\text{M} = \text{Nb}, \text{Ta}; \text{M}' = \text{Mn, Re}; n = 1, 2$ ). *Inorg. Chem.* **2001**, *40* (11), 2582–2586.
- (40) Zhu, Z. K.; Zhang, J.; Cong, Y. C.; Ge, R.; Li, Z.; Li, X. X.; Zheng, S. T. Two Giant Calixarene-Like Polyoxoniobate Nanocups  $\{\text{Cu}_{12}\text{Nb}_{120}\}$  and  $\{\text{Cd}_{16}\text{Nb}_{128}\}$  Built from Mixed Macroyclic Cluster Motifs. *Angew. Chem. Int. Edit.* **2022**, *61* (7), DOI: 10.1002/anie.202113381.
- (41) Martin, N. P.; Nyman, M. Directional Bonding in Decaniobate Inorganic Frameworks. *Angew. Chem. Int. Edit.* **2021**, *60* (2), 954–960.
- (42) Lai, R. D.; Zhang, J.; Li, X. X.; Zheng, S. T.; Yang, G. Y. Assemblies of Increasingly Large Ln-Containing Polyoxoniobates and Intermolecular Aggregation-Disaggregation Interconversions. *J. Am. Chem. Soc.* **2022**, *144* (42), 19603–19610.
- (43) Nyman, M.; Powers, C. R.; Bonhomme, F.; Alam, T. M.; Maginn, E. J.; Hobbs, D. T. Ion-Exchange Behavior of One-Dimensional Linked Dodecaniobate Keggin Ion Materials. *Chem. Mater.* **2008**, *20* (7), 2513–2521.
- (44) Anderson, T. M.; Alam, T. M.; Rodriguez, M. A.; Bixler, J. N.; Xu, W. Q.; Parise, J. B.; Nyman, M. Cupric Silicoibate. Synthesis and Solid-State Studies of a Pseudosandwich-Type Heteropolyanion. *Inorg. Chem.* **2008**, *47* (17), 7834–7839.
- (45) Nyman, M.; Bonhomme, F.; Alam, T. M.; Parise, J. B.; Vaughan, G. M. B.  $[\text{SiNb}_{12}\text{O}_{40}]^{16^-}$  and  $[\text{GeNb}_{12}\text{O}_{40}]^{16^-}$ : Highly Charged Keggin Ions with Sticky Surfaces. *Angew. Chem. Int. Edit.* **2004**, *43* (21), 2787–2792.
- (46) Nyman, M.; Celestian, A. J.; Parise, J. B.; Holland, G. P.; Alam, T. M. Solid-State Structural Characterization of a Rigid Framework of Lacunary Heteropolyaniobates. *Inorg. Chem.* **2006**, *45* (3), 1043–1052.
- (47) Martin, N. P.; Petrus, E.; Segado, M.; Arteaga, A.; Zakharov, L. N.; Bo, C.; Nyman, M. Strategic Capture of the  $\{\text{Nb}-7\}$  Polyoxometalate. *Chem.—Eur. J.* **2019**, *25* (45), 10580–10584.
- (48) Graeber, E. J.; Morosin, B. The Molecular Configuration of The Decaniobate Ion  $(\text{Nb}_{10}\text{O}_{28})^{6-x^-}$ . *Acta Crystallogr.* **1977**, *B33*, 2137–2143.
- (49) Marek, K. A. *Polyoxoniobates: How Solution Chemistry Helps to Understand the Solid State*. PhD Thesis, UIUC, 2001.
- (50) Villa, E. M.; Ohlin, C. A.; Balogh, E.; Anderson, T. M.; Nyman, M. D.; Casey, W. H. Reaction Dynamics of the Decaniobate Ion  $[\text{H}_x\text{Nb}_{10}\text{O}_{28}]^{(6-x)^-}$  in Water. *Angew. Chem. Int. Edit.* **2008**, *47* (26), 4844–4846.
- (51) Bontchev, R. P.; Nyman, M. Evolution of Polyoxoniobate Cluster Anions. *Angew. Chem. Int. Edit.* **2006**, *45* (40), 6670–6672.
- (52) Miras, H. N.; Wilson, E. F.; Cronin, L. Unravelling the Complexities of Inorganic and Supramolecular Self-Assembly in Solution with Electrospray and Cryospray Mass Spectrometry. *Chem. Commun.* **2009**, No. 11, 1297–1311.
- (53) Nyman, M.; Rodriguez, M. A.; Campana, C. F. Self-Assembly of Alkali-Uranyl-Peroxide Clusters. *Inorg. Chem.* **2010**, *49* (17), 7748–7755.
- (54) Gaukas, N. H.; Dale, S. M.; Raeder, T. M.; Toresen, A.; Holmestad, R.; Glaum, J.; Einarsrud, M. A.; Grande, T. Controlling Phase Purity and Texture of  $\text{K}_{0.5}\text{Na}_{0.5}\text{NbO}_3$  Thin Films by Aqueous Chemical Solution Deposition. *Materials* **2019**, *12* (13), DOI: 10.3390/ma12132042.
- (55) Rahman, T.; Martin, N. P.; Jenkins, J. K.; Elzein, R.; Fast, D. B.; Addou, R.; Herman, G. S.; Nyman, M.  $\text{Nb}_2\text{O}_5$ ,  $\text{LiNbO}_3$ , and  $(\text{Na}, \text{K})\text{NbO}_3$  Thin Films from High-Concentration Aqueous Nb-Polyoxometalates. *Inorg. Chem.* **2022**, *61* (8), 3586–3597.
- (56) Huang, P.; Qin, C.; Su, Z. M.; Xing, Y.; Wang, X. L.; Shao, K. Z.; Lan, Y. Q.; Wang, E. B. Self-Assembly and Photocatalytic Properties of Polyoxoniobates:  $\{\text{Nb}_{24}\text{O}_{72}\}$ ,  $\{\text{Nb}_{32}\text{O}_{96}\}$ , and  $\{\text{K}_{12}\text{Nb}_{96}\text{O}_{288}\}$  Clusters. *J. Am. Chem. Soc.* **2012**, *134* (34), 14004–14010.
- (57) Lai, R. D.; Zhu, Z. K.; Wu, Y. L.; Sun, Y. Q.; Sun, C.; Li, X. X.; Zheng, S. T. Proton-Conductive Polyoxometalate Architectures Constructed from Lanthanide-Incorporated Polyoxoniobate Cages. *Inorg. Chem.* **2022**, *61* (51), 21047–21054.
- (58) Yu, H.; Lin, Y. D.; Huang, S. L.; Li, X. X.; Sun, C.; Zheng, S. T. Photochromic Polyoxoniobates with Photoinduced "D-F-a" Electron Transfer Mechanism. *Angew. Chem. Int. Edit.* **2023**, *62* (26), DOI: 10.1002/anie.202302111.
- (59) Lee, U.; Joo, H. C.; Park, K. M.; Mal, S. S.; Kortz, U.; Keita, B.; Nadjo, L. Facile Incorporation of Platinum(IV) into Polyoxometalate Frameworks: Preparation of  $[(\text{H}_2\text{PtV}_9\text{O}_{28})]^{5^-}$  and Characterization by Pt-195 NMR Spectroscopy. *Angew. Chem. Int. Edit.* **2008**, *47* (4), 793–796.
- (60) Konaka, S.; Ozawa, Y.; Yagasaki, A.  $[\text{HTeV}_9\text{O}_{28}]^{4^-}$ : A New Vanadotellurate with Decavanadate Structure. *Inorg. Chem. Commun.* **2008**, *11* (10), 1267–1269.
- (61) Kostenkova, K.; Arhouna, Z.; Postal, K.; Rajan, A.; Kortz, U.; Nunes, G. G.; Crick, D. C.; Crans, D. C.  $\text{Pt}^{\text{IV}}$  or  $\text{Mo}^{\text{VI}}$ -Substituted Decavanadates Inhibit the Growth of Mycobacterium Smegmatis. *J. Inorg. Biochem.* **2021**, *217*, DOI: 10.1016/j.jinorgbio.2021.111356.
- (62) Son, J. H.; Ohlin, C. A.; Casey, W. H. Highly Soluble Iron- and Nickel-Substituted Decaniobates with Tetramethylammonium Counterions. *Dalton Transac* **2013**, *42* (21), 7529–7533.
- (63) Son, J. H.; Wang, J. R.; Casey, W. H. Structure, Stability and Photocatalytic  $\text{H}_2$  Production by Cr-, Mn-, Fe-, Co-, and Ni-Substituted Decaniobate Clusters. *Dalton Transac* **2014**, *43* (48), 17928–17933.
- (64) Son, J. H.; Ohlin, C. A.; Casey, W. H. A New Class of Soluble and Stable Transition-Metal-Substituted Polyoxoniobate:  $[\text{Cr}_2(\text{OH})_4\text{Nb}_{10}\text{O}_{30}]^{8^-}$ . *Dalton Transac* **2012**, *41* (41), 12674–12677.
- (65) Nyman, M.; Criscenti, L. J.; Bonhomme, F.; Rodriguez, M. A.; Cygan, R. T. Synthesis, Structure, and Molecular Modeling of a Titanoniobate Isopolyanion. *J. Solid State Chem.* **2003**, *176* (1), 111–119.
- (66) Perezbenito, J. F.; Brillas, E.; Pouplana, R. Identification of a Soluble Form of Colloidal Manganese(IV). *Inorg. Chem.* **1989**, *28* (3), 390–392.
- (67) Babes, L.; Denizot, B.; Tanguy, G.; Le Jeune, J. J.; Jallet, P. Synthesis of Iron Oxide Nanoparticles Used as MRI Contrast Agents: A Parametric Study. *J. Colloid Interface Sci.* **1999**, *212* (2), 474–482.
- (68) Villa, E. M.; Ohlin, C. A.; Casey, W. H. Oxygen-Isotope Exchange Rates for Three Isostructural Polyoxometalate Ions. *J. Am. Chem. Soc.* **2010**, *132* (14), 5264–5272.
- (69) Rahman, T.; Petrus, E.; Segado, M.; Martin, N. P.; Palys, L. N.; Rambaran, M. A.; Ohlin, C. A.; Bo, C.; Nyman, M. Predicting the Solubility of Inorganic Ions Pairs in Water. *Angew. Chem. Int. Edit.* **2022**, *61* (19), DOI: 10.1002/anie.202117839.
- (70) Maekawa, M.; Ozawa, Y.; Yagasaki, A. Icosaniobate: A New Member of the Isoniobate Family. *Inorg. Chem.* **2006**, *45* (24), 9608–9609.
- (71) Rahman, T.; Petrus, E.; Segado, M.; Martin, N. P.; Palys, L. N.; Rambaran, M. A.; Ohlin, C. A.; Bo, C.; Nyman, M. Predicting the Solubility of Inorganic Ion Pairs in Water. *Angew. Chem.* **2022**, *134* (19), No. e202117839.
- (72) Petrus, E.; Segado-Centellas, M.; Bo, C. R. Computational Prediction of Speciation Diagrams and Nucleation Mechanisms: Molecular Vanadium, Niobium, and Tantalum Oxide Nanoclusters in Solution. *Inorg. Chem.* **2022**, *61* (35), 13708–13718.